Letter

Chaos-assisted turbulence in spinor Bose-Einstein condensates

Jongmin Kim,[1,*] Jongheum Jung,[1,*] Junghoon Lee,[1] Deokhwa Hong,[1] and Y. Shin[1,2,†]
[1]Department of Physics and Astronomy, Seoul National University, Seoul 08826, Korea
[2]Institute of Applied Physics, Seoul National University, Seoul 08826, Korea

(Received 1 March 2024; accepted 8 July 2024; published 8 August 2024)

We present a turbulence-sustaining mechanism in a spinor Bose-Einstein condensate, which is based on the chaotic nature of internal spin dynamics. Magnetic driving induces a complete chaotic evolution of the local spin state, thereby continuously randomizing the spin texture of the condensate to maintain the turbulent state. We experimentally demonstrate the onset of turbulence in the driven condensate as the driving frequency changes and show that it is consistent with the regular-to-chaotic transition of the local spin dynamics. This chaos-assisted turbulence establishes the spin-driven spinor condensate as an intriguing platform for exploring quantum chaos and related superfluid turbulence phenomena.

DOI: 10.1103/PhysRevResearch.6.L032030

Turbulence, a ubiquitous phenomenon in fluids, poses a major challenge in physics owing to its complexity [1]. To effectively investigate this phenomenon, it is essential to generate turbulence in a controlled manner. Various existing methods, such as moving grids [2–4], impinging jets [5,6], and rotating drums [7–9], have provided valuable insights into the different aspects of turbulent states, highlighting the strong connection between the generation method and flow dynamics. However, these approaches are primarily based on local or anisotropic external forces and inertial energy cascades [10–12], which might limit the possibilities of exploring novel properties of turbulent states. Here, we propose an alternative approach to generate turbulence by harnessing the intrinsic chaos within the fluid itself. By utilizing the unpredictable and sensitive nature of chaotic systems, this method introduces energy directly into the flow through self-amplifying mechanisms similar to the stretching and folding of fluid elements [13]. This chaos-based method holds the potential for improved mixing and homogeneous, isotropic energy injection, thereby offering the opportunity to explore previously uncharted turbulent behaviors.

In this Letter, we present a case study of chaos-assisted turbulence with spin-1 atomic Bose-Einstein condensates (BECs). This system is a superfluid with internal spin degrees of freedom that presents a departure from conventional superfluid dynamics. The order parameter of the superfluid can be expressed as $\Psi = \sqrt{n}e^{i\varphi}\boldsymbol{\zeta}$, where n is the superfluid density, φ is the superfluid phase, and $\boldsymbol{\zeta}$ is the spinor for the spin state. Due to the intricate relation between the superfluid phase and the spin rotation [14], mass superflow is associated not only with the spatial variations of φ but also with those of $\boldsymbol{\zeta}$, i.e., with the spin texture. The superfluid velocity and its vorticity are given by

$$\begin{aligned} \boldsymbol{v}_s &= \frac{\hbar}{m}(\nabla\varphi - i\boldsymbol{\zeta}^\dagger\nabla\boldsymbol{\zeta}), \\ \nabla\times\boldsymbol{v}_s &= -\frac{i\hbar}{m}\nabla\boldsymbol{\zeta}^\dagger\times\nabla\boldsymbol{\zeta}, \end{aligned} \tag{1}$$

where m is the particle mass and $\hbar$ is the reduced Planck constant, $h/2\pi$. Therefore, a mass superflow can be generated by manipulating the spin texture in space.

The situation considered in this Letter is that the local dynamics of $\boldsymbol{\zeta}$ is in a classically chaotic regime. Then, because of the hypersensitivity on initial conditions, small spatial fluctuations in a superfluid, even starting with a uniform spin texture, would develop into complex spatial variations of the spin states over time evolution, leading to an irregular spin texture. If the spin texture is kept irregular because of the chaotic nature of the local spin dynamics, the resulting turbulent flow in the superfluid would be sustained. This is a scenario of the aforementioned chaos-assisted turbulence generation.

Recently, stationary turbulent states have been observed in a spin-1 BEC when it is subjected to continuous radio-frequency (rf) magnetic fields [15,16]. Under specific driving conditions, the turbulence attains its maximum intensity, accompanied by an isotropic spin composition. Although the rf magnetic field, aided by field noise, has been identified as the driving force, the mechanism that sustains the generated turbulence while maintaining the isotropic spin nature has remained unclear. In this Letter, through numerical simulations and experimental validation, we demonstrate that the applied magnetic field induces chaotic motion within local spin states, thus sustaining the turbulent state. This finding concretizes the notion of chaos-assisted turbulence generation, particularly in a superfluid system, paving the way for a deeper understanding and control of this complex and fascinating phenomenon.

*These authors contributed equally to this work.
†Contact author: yishin@snu.ac.kr

Our superfluid system is a BEC of ^{23}Na atoms in the $F = 1$ hyperfine state with antiferromagnetic interactions [17,18]. A uniform external magnetic field of B_z is applied along $\hat{\boldsymbol{z}}$, and for spin driving, an rf magnetic field with oscillating frequency of ω is applied along the transverse direction. In a mean-field description, neglecting the spatial modes of the BEC and taking the rotating-wave approximation, the local dynamics of the spin state $\boldsymbol{\zeta} = (\zeta_{+1}, \zeta_0, \zeta_{-1})^{\mathrm{T}}$ is described by the following Hamiltonian per particle,

$$H_s = \hbar\delta f_z - \hbar\Omega f_x + q\boldsymbol{\zeta}^\dagger \mathrm{f}_z^2 \boldsymbol{\zeta} + \varepsilon_s |\boldsymbol{f}|^2, \tag{2}$$

where $\mathbf{f} = (\mathrm{f}_x, \mathrm{f}_y, \mathrm{f}_z)$ are the spin operators of the spin-1 system and $\boldsymbol{f} = \boldsymbol{\zeta}^\dagger \mathbf{f} \boldsymbol{\zeta}$ is the spin vector with $f_{x,y,z}$ representing the magnetizations in the x, y, and z directions, respectively. $\delta = \omega - \omega_0$ is the frequency detuning of the rf magnetic field from the Larmor frequency $\omega_0 = \frac{1}{2}\mu_{\mathrm{B}} B_z/\hbar$ with μ_{B} being the Bohr magneton, Ω is the Rabi frequency of the rf field, and q denotes the quadratic Zeeman energy. The last term represents the energy of spin interaction, which introduces nonlinearity to the system.

When the energy scales of ε_s, q, and $\hbar\Omega$ are comparable and $\delta = 0$, it is known that the spin dynamics of the Hamiltonian H_s becomes chaotic [19,20]. Here, we investigate a magnetic driving scheme where the external magnetic field B_z is modulated such that $\delta(t) = \delta_0 + D\sin(2\pi\nu t + \phi)$ [Fig. 1(a)]. This field modulation breaks the energy conservation constraint, possibly enhancing the chaoticity of the system and facilitating complete randomization of the spin state [21,22].

To demonstrate the chaotic behavior of the spin system, we numerically investigate the time evolution of an ensemble of spin states, $\mathcal{E}$, and characterize it in the coordinate space of magnetization $\boldsymbol{f}$. The ensemble $\mathcal{E}$ consists of 128^2 spin states, whose initial states are constructed from the $m_F = 0$ state $[\boldsymbol{\zeta} = (0, 1, 0)^{\mathrm{T}}]$ with small Gaussian random noise added [23], so $\boldsymbol{f} \approx \mathbf{0}$. The system parameters are set to $\varepsilon_s/h = 45$ Hz, $q/h = 47$ Hz, $\Omega/2\pi = 200$ Hz, and $\nu = 60$ Hz. Figure 1(b) shows the $\boldsymbol{f}$ distributions of the ensemble after the evolution of 1 s for various sets of driving parameters $\{\delta_0, D\}$. Without field modulation ($D = 0$) and for small δ_0 (case I), the magnetization is dispersed on the plane perpendicular to the linear Zeeman field, but far from fully randomized. Meanwhile, when subjected to the field modulation, the ensemble spreads over a broader region of the magnetization space (cases II and III), implying the enhanced spin mixing of the system [23]. For large δ_0 (case IV), the spin dynamics is observed to be regular.

As a proxy of the randomness of the spin states in $\mathcal{E}$, we estimate a trace distance,

$$\Delta^{(2)} \equiv \tfrac{1}{2}\left|\left|\rho_{\mathcal{E}}^{(2)} - \rho_{\mathrm{Haar}}^{(2)}\right|\right|_1, \tag{3}$$

where $\rho_{\mathcal{E}}^{(2)} = \sum_{\zeta\sim\mathcal{E}} (\boldsymbol{\zeta}\boldsymbol{\zeta}^\dagger)^{\otimes 2}$ is the second momentum of the ensemble [24], and $\rho_{\mathrm{Haar}}^{(2)}$ is that of the Haar random ensemble $\mathcal{E}_{\mathrm{Haar}}$, which is a unitarily invariant, maximally randomized ensemble of the spin-1 system [22,25,26]. Here, $||\cdot||_1$ denotes the trace norm, and $0 \leqslant \Delta^{(2)} \leqslant 1$ represents how much different the ensemble $\mathcal{E}$ is from $\mathcal{E}_{\mathrm{Haar}}$, i.e., a smaller $\Delta^{(2)}$ indicates that $\mathcal{E}$ is more randomized. Figure 1(c) shows the evolution curves of $\Delta^{(2)}$ for the different driving parameters.

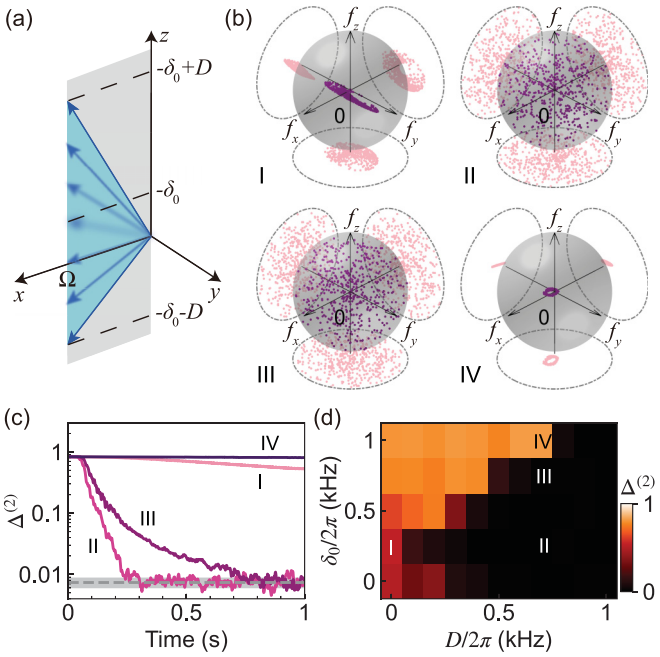

FIG. 1. Chaotic spin dynamics in a spinor Bose-Einstein condensate under magnetic field modulations. (a) The linear Zeeman field in Eq. (2) oscillates as $\Omega\hat{\mathbf{x}} - \delta(t)\hat{\mathbf{z}}$ with $\delta(t) = \delta_0 + D\sin(2\pi\nu t + \phi)$ and $\nu = 60$ Hz. (b) Magnetization, $\boldsymbol{f} = (f_x, f_y, f_z)$, distributions of a spin state ensemble after 1-s spin driving for four different sets of driving parameters: (I) $\{\delta_0, D\}/2\pi = \{250, 0\}$, (II) $\{250, 700\}$, (III) $\{750, 700\}$, and (IV) $\{1000, 700\}$ Hz. The ensemble consists of 128^2 spin states, which initially have $\boldsymbol{f} \approx \mathbf{0}$ (see text for details). Pink points show the projections of $\boldsymbol{f}$ along the xy, yz, and zx planes. (c) Time evolution of the second-momentum trace distances $\Delta^{(2)}$ between the spin state ensemble and the Haar random ensemble for (I)–(IV). The dashed line represents the expectation value for a set of 128^2 spin states sampled from the Haar ensemble. (d) $\Delta^{(2)}$ after 1-s spin driving as a function of δ_0 and D.

In a specific driving condition, $\mathcal{E}$ becomes fully randomized as $\Delta^{(2)} \simeq 0$. In Fig. 1(d), the value of $\Delta^{(2)}$ after 1 s of spin driving is displayed in the plane of δ_0 and D. Interestingly, the dynamic behavior of the system exhibits a sudden transition from chaotic to regular as δ_0 exceeds a threshold value δ_{th}. The value of δ_{th} is found to be linearly proportional to the magnitude of field modulation as $\delta_{\mathrm{th}} \simeq D$, highlighting the role of field modulation in the randomization of the spin state. This also shows that, as the direction of the linear Zeeman field varies significantly during the driving [Fig. 1(a)], meeting the resonance condition of $\delta = 0$ is important to be chaotic. The nature of the sudden transition warrants further investigation.

We extend our discussion to the dynamics of a BEC with spatial extent, e.g., in two dimensions. Here, the spinor condensate can be viewed as the spatial array of the local nonlinear spin subsystems that are coupled to their neighbors. We numerically calculate the system's evolution using spin-1 Gross-Pitaevskii equations (GPEs) [23,27]. The condensate is initially prepared in the $m_F = 0$ state with quantum noise, where the noise is determined in accordance with the truncated Wigner approximation [23,28]. An irregular spin texture develops under spin driving, e.g., with $\delta_0/2\pi = 500$ Hz and

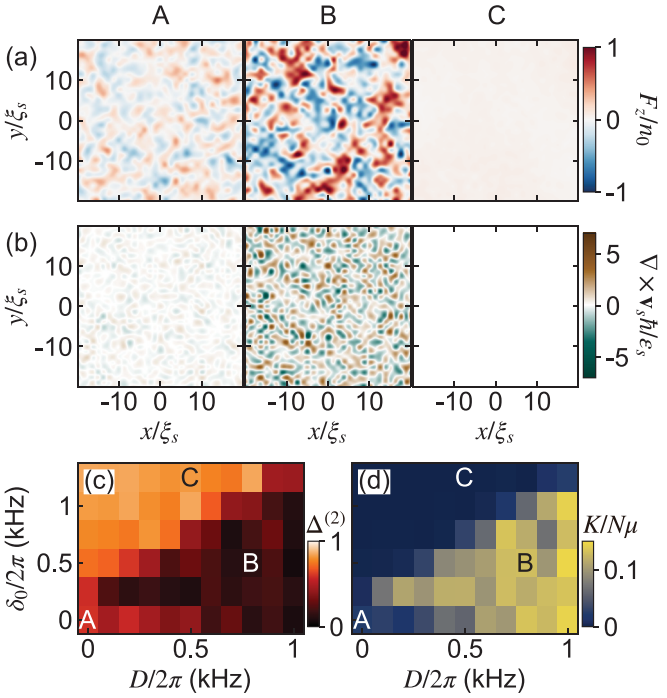

FIG. 2. Turbulence generation in a spinor BEC by spin driving. (a) Magnetization F_z and (b) vorticity $\nabla \times \boldsymbol{v}_s$ distributions in a two-dimensional BEC after 1-s spin driving for three different driving conditions: (A) $\{\delta_0, D\}/2\pi = \{0, 0\}$, (B) $\{500, 800\}$, and (C) $\{1250, 500\}$ Hz. $F_z = nf_z$ is the density of magnetization along the z direction and $\boldsymbol{v}_s$ is the superflow velocity. n_0 is the mean particle density, ε_s denotes the spin interaction energy scale, and ξ_s is the spin healing length. (c) $\Delta^{(2)}$ and (d) kinetic energy K, as functions of δ_0 and D. N is the total particle number and μ denotes the chemical potential of the BEC.

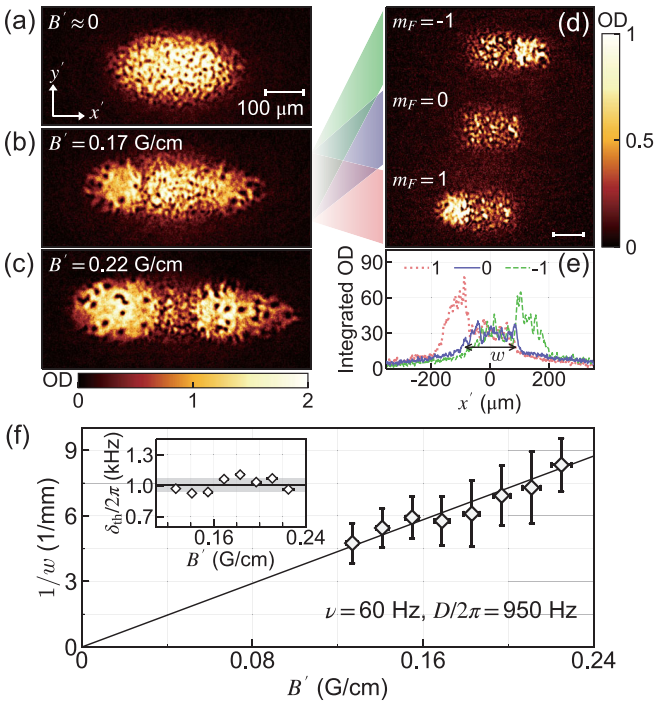

FIG. 3. Observation of the turbulence onset in a driven spinor BEC. (a)–(c) Time-of-flight images of BECs after spin driving for 2 s with $\delta_0 = 0$, $D/2\pi = 950$ Hz, $\nu = 60$ Hz, and $\phi = 0$. Turbulence appears as irregular density patterns in the freely expanding BECs. A magnetic field gradient B' was applied along the x' direction during spin driving. (d) Image after Stern-Gerlach spin separation for $B' = 0.17$ G/cm. The deformation of the clouds due to separation is compensated by perspective transformation [23]. (e) Integrated density profiles of the three spin components. The width w of the spin turbulence region was determined from the density distribution of the $m_F = 0$ component. (f) $1/w$ as a function of B'. Each data point was obtained from the 20–30 measurements and its error bar indicates their standard deviation. The solid line is a linear line of $w^{-1} = \alpha B'$ with $\alpha = 3.7 \times 10^4$/G, fit to the data. The inset shows the values of $\delta_{\rm th} = \frac{\mu_B}{4\hbar} B' w$. The horizontal line and the shaded region indicate their mean and standard deviation, respectively.

$D/2\pi = 800$ Hz [Fig. 2(a), case B]. The irregular spin texture implies turbulent superflow in the spinor BEC, as verified by the vorticity distribution of the superfluid velocity in Fig. 2(b).

The range of driving parameters for the generation of turbulence is well aligned with that for the chaotic spin dynamics. In Figs. 2(c) and 2(d), we plot the trace distance $\Delta^{(2)}$ and the kinetic energy K of the system in the δ_0-D plane, respectively. Here, $\Delta^{(2)}$ is measured from the spin state ensemble $\mathcal{E}$ obtained by position projection of the condensate, such that each spin state of the ensemble is associated with a local position and weighted by the density at the position [16], and the kinetic energy is calculated as $K = \int d^2\boldsymbol{r}\Psi^\dagger(-\frac{\hbar^2}{2m}\nabla^2)\Psi$. The relationship of $\delta_{\rm th} \simeq D$ is still observed as in Fig. 1(d), which clearly demonstrates that the turbulence generation originates from chaotic spin dynamics. Meanwhile, the value of $\Delta^{(2)}$ for turbulent BEC appears to be relatively higher than the corresponding value in Fig. 1(d). It is attributed to the energy dissipation process through spin-wave relaxation [15], which would homogenize the spin texture. Further characterization of the velocity fields of the turbulent BEC is provided in [23], where a $-5/3$ power-law scaling was observed in the incompressible part of the kinetic energy [29].

Next, we conduct an experimental verification of the turbulence generation mechanism assisted by chaotic spin dynamics. We prepare a BEC consisting of about 3.5×10^6 ^{23}Na atoms in the $|F = 1, m_F = 0\rangle$ state. The BEC is trapped in an optical dipole trap of highly oblate geometry and its Thomas-Fermi (TF) radii are $(R_{x'}, R_{y'}, R_{z'}) \approx (160, 75, 1.6)$ μm, where x', y', and z' denote spatial coordinates. For the peak atomic density at the trap center, the spin interaction energy is $\varepsilon_s \approx h \times 53$ Hz [30] and the spin healing length $\xi_s = \hbar/\sqrt{2m\varepsilon_s} \approx 2.0$ μm, comparable to the thickness of the sample. A uniform external magnetic field of $B_z \approx 0.41$ G is applied along $\hat{\boldsymbol{z}} = (-\hat{\boldsymbol{x}}' + \hat{\boldsymbol{y}}')/\sqrt{2}$, giving $\omega_0 \approx 2\pi \times 291$ kHz and $q \approx h \times 47$ Hz. An rf magnetic field is applied along $\hat{\boldsymbol{y}}'$ with $\Omega = 2\pi \times 150$ Hz. The external magnetic field B_z is sinusoidally modulated at $\nu = 60$ Hz with a variable magnitude of less than a few mG.

Figure 3(a) shows an optical density (OD) image of a BEC, taken along the $\hat{\boldsymbol{z}}'$ direction after a 18-ms time of flight [31]. The BEC was spin driven for 2 s with $\delta_0 = 0$ and $D/2\pi = 950$ Hz. A stationary turbulent state appears in the driven BEC, manifested by an irregular density distribution

that arises after free expansion from the chaotic velocity field of the driven condensate. Furthermore, the turbulent BEC exhibits equal populations in all three spin states. The spin isotropy of the turbulent BEC was demonstrated in Ref. [15] by showing that the populations of the three spin states are equal regardless of the quantization axis.

We investigate how the frequency detuning δ_0 of the rf driving field affects turbulence generation by conducting a similar experiment with an additional magnetic field gradient B' applied along the long axis of the condensate. This field gradient renders the frequency detuning of the rf driving spatially varying across the condensate as $\delta_0(x') = (\frac{1}{2}\mu_B B' x')/\hbar$. We observe that spin-isotropic turbulence occurs within a central region of the condensate [Figs. 3(b) and 3(c)], whose spatial extent decreases as B' increases, implying the existence of a range of δ_0 effective for the generation of turbulence.

The image obtained after Stern-Gerlach spin separation reveals that the turbulent region is positioned between two ferromagnetic domains with opposite magnetizations [Fig. 3(d)]. For high $|\delta|$, the ground state of the driven BEC is ferromagnetic owing to the large Zeeman energy. As the BEC is driven, the ferromagnetic domains gradually appear at both ends of the condensate and reach saturation in the steady state, containing vortices [23]. The interface between the turbulent region and the ferromagnetic domains is clearly defined, showing sudden changes in density for the different spin components [Figs. 3(d) and 3(e)]. This allows us to reliably determine the turbulent region from the density distribution of the $m_F = 0$ component.

We measure the spatial extent w of the spin-isotropic turbulent region along the direction of the field gradient, and find that its inverse is proportional to the magnitude of the field gradient [Fig. 3(f)]. This means that the threshold value of δ_0 for turbulence generation is consistently determined as $\delta_{\rm th} = \delta_0(\frac{w}{2}) = \mu_B B' w/4\hbar$. The presence of such a threshold detuning is in excellent agreement with the numerical results shown in Fig. 2, providing clear evidence of the regular-to-chaotic transition in the driven spinor BEC system.

The relationship of $\delta_{\rm th}$ and the magnitude D of the field modulations is investigated (Fig. 4). As D increases, in general, $\delta_{\rm th}$ increases, which is consistent with the expected behavior of the spin dynamics. However, we observe that a turbulent region is formed even in the absence of field modulations, indicating a threshold detuning of $\delta_{\rm th,0} = 0.74(9)$ kHz for $D = 0$. We find that it is caused by ambient magnetic field fluctuations, which amounts to about 1 mG [15]. Magnetic field noises are likely generated by current ripples in the magnetic coils that leak from the 60-Hz ac power line. In fact, for $\nu = 60$ Hz, $\delta_{\rm th}$ shows a sinusoidal dependence on the phase ϕ of the external field modulation [Fig. 4(c)], and it arises from interference with the background field component oscillating at the same frequency.

Taking into account such ambient field fluctuation effects, we present an empirical model of the threshold detuning as

$$\delta_{\rm th}^2 = \beta_\nu^2[D^2 + 2DD_\nu \cos(\phi - \phi_\nu)] + \delta_{\rm th,0}^2, \qquad (4)$$

where D_ν and ϕ_ν represent the amplitude and phase, respectively, of the background field component that coherently

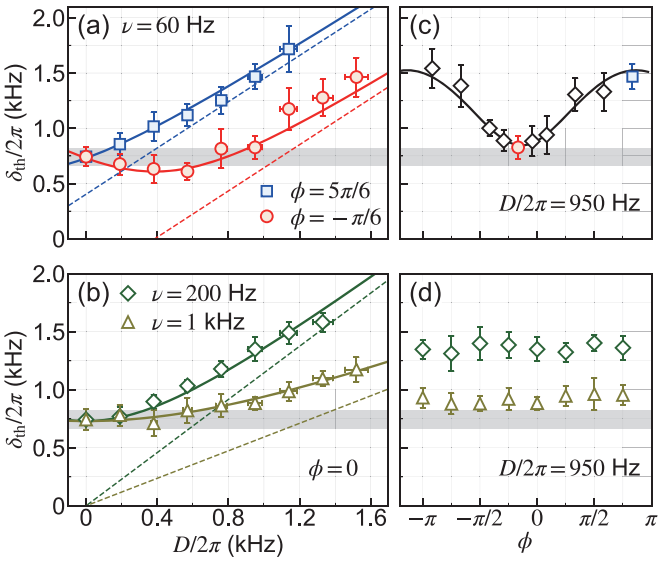

FIG. 4. Threshold detuning $\delta_{\rm th}$ of the spin driving for turbulence generation. Dependence of $\delta_{\rm th}$ on the driving amplitude D for (a) $\nu =$ 60 Hz, (b) 200 Hz and 1 kHz. The gray horizontal lines indicate the threshold detuning value of $\delta_{\rm th,0}/2\pi = 0.74(9)$ kHz due to ambient field noise. Corresponding $\delta_{\rm th}$ data for different modulation phases ϕ with $D/2\pi = 1$ kHz for (c) $\nu = 60$ Hz, (d) 200 Hz and 1 kHz. Each data point indicates the mean value of 10–20 measurements, and its error bar is the standard deviation of the measurements. The solid lines in (a) and (c) are the model curves of Eq. (4) with the parameter values of $\{\beta_\nu, D_\nu/2\pi, \phi_\nu\} = \{1.05, 0.39\ \text{kHz}, 0.86\pi\}$, which were determined from a model fit to the data in (c). The solid lines in (b) are model curves fit to the data with $D_\nu = 0$. The dashed lines indicate the corresponding model curves with $\delta_{\rm th,0} = 0$.

oscillates at frequency ν, and β_ν denotes the proportionality of $\delta_{\rm th}$ to the field modulation [23]. Our measurement results of $\delta_{\rm th}$ for various D and ϕ are well described by the model [Fig. 4(a)], suggesting $D_\nu/2\pi = 0.39(5)$ kHz and $\beta_\nu = 1.05(6)$ for $\nu = 60$ Hz. In Fig. 4(b), we show additional measurement data of $\delta_{\rm th}$ for $\nu = 200$ Hz and 1 kHz, where the model curve fitting to the data provides $D_\nu \approx 0$ and $\beta_\nu =$ 1.15(4) and 0.59(4), respectively. It is evident that when the modulation frequency surpasses the energy scales relevant to the system, the efficiency of the mixing caused by the external field modulation is reduced.

In conclusion, we have presented a turbulence generation mechanism based on chaos and demonstrated it with the spinor BEC system under magnetic field driving. The presence of the threshold frequency detuning $\delta_{\rm th}$ and its linear relationship with D were demonstrated, in excellent agreement with the predicted regular-to-chaotic transition. The stationary turbulence state of the spinor BEC provides interesting opportunities to explore nonequilibrium superfluid dynamics. An important next step is to compare this chaos-assisted turbulence with conventional hydrodynamic turbulence, where energy is injected on a certain length scale and an inertial energy cascade follows [10–12,23]. The immediate extension of this work would be to quantify the spin texture [32,33] and the mechanisms of energy transfer and dissipation [29,34] of the turbulent BEC. Given that our driven system exhibits spatiotemporally chaotic flow induced by its

internal spin dynamics, it would be interesting to explore its possible connection to *active* turbulence [35,36], which is self-driven turbulence by spontaneous flow instability.

This work was supported by the National Research Foundation of Korea (Grants No. NRF-2023R1A2C3006565 and No. NRF-2023M3K5A1094811).

[1] R. P. Feynmann, R. B. Leighton, and M. Sands, *The Feynman Lectures on Physics* (Addison-Wesley, Reading, MA, 1971), Vol. I.

[2] M. Hideharu, Realization of a large-scale turbulence field in a small wind tunnel, Fluid Dyn. Res. **8**, 53 (1991).

[3] L. Mydlarski and Z. Warhaft, On the onset of high-Reynolds-number grid-generated wind tunnel turbulence, J. Fluid Mech. **320**, 331 (1996).

[4] M. R. Smith, R. J. Donnelly, N. Goldenfeld, and W. F. Vinen, Decay of vorticity in homogeneous turbulence, Phys. Rev. Lett. **71**, 2583 (1993).

[5] D. Cooper, D. C. Jackson, B. E. Launder, and G. X. Liao, Impinging jet studies for turbulence model assessment—I. Flow-field experiments, Int. J. Heat Mass Transfer **36**, 2675 (1993).

[6] M. Kim, D. Schanz, M. Novara, P. Godbersen, E. Yeom, and A. Schröder, Experimental study on flow and turbulence characteristics of jet impinging on cylinder using three-dimensional Lagrangian particle tracking velocimetry, Sci. Rep. **13**, 10929 (2023).

[7] G. Seiden and P. J. Thomas, Complexity, segregation, and pattern formation in rotating-drum flows, Rev. Mod. Phys. **83**, 1323 (2011).

[8] V. Eltsov, R. de Graaf, R. Hanninen, M. Krusius, R. Solntsev, V. L'vov, A. Golov, and P. Walmsley, Turbulent dynamics in rotating helium superfluids, Prog. Low Temp. Phys. **16**, 45 (2009).

[9] M. Brunet, B. Gallet, and P.-P. Cortet, Shortcut to geostrophy in wave-driven rotating turbulence: The quartetic instability, Phys. Rev. Lett. **124**, 124501 (2020).

[10] W. F. Vinen and J. J. Niemela, Quantum turbulence, J. Low Temp. Phys. **128**, 167 (2002).

[11] N. Navon, A. L. Gaunt, R. P. Smith, and Z. Hadzibabic, Emergence of a turbulent cascade in a quantum gas, Nature (London) **539**, 72 (2016).

[12] A. Alexakis and L. Biferale, Cascades and transitions in turbulent flows, Phys. Rep. **767-769**, 1 (2018).

[13] L. E. Reichl, *The Transition to Chaos: Conservative Classical Systems and Quantum Manifestations*, 2nd ed. (Springer, New York, 2004).

[14] Y. Kawaguchi and M. Ueda, Spinor Bose–Einstein condensates, Phys. Rep. **520**, 253 (2012).

[15] D. Hong, J. Lee, J. Kim, J. H. Jung, K. Lee, S. Kang, and Y. Shin, Spin-driven stationary turbulence in spinor Bose-Einstein condensates, Phys. Rev. A **108**, 013318 (2023).

[16] J. H. Jung, J. Lee, J. Kim, and Y. Shin, Random spin textures in turbulent spinor Bose-Einstein condensate, Phys. Rev. A **108**, 043309 (2023).

[17] F. Zhou, Quantum spin nematic states in Bose–Einstein condensates, Int. J. Mod. Phys. B **17**, 2643 (2003).

[18] S. W. Seo, S. Kang, W. J. Kwon, and Y. I. Shin, Half-quantum vortices in an antiferromagnetic spinor Bose-Einstein condensate, Phys. Rev. Lett. **115**, 015301 (2015).

[19] M. Rautenberg and M. Gärttner, Classical and quantum chaos in a three-mode bosonic system, Phys. Rev. A **101**, 053604 (2020).

[20] B. Evrard, A. Qu, J. Dalibard, and F. Gerbier, From many-body oscillations to thermalization in an isolated spinor gas, Phys. Rev. Lett. **126**, 063401 (2021).

[21] J. Choi, A. L. Shaw, I. S. Madjarov, X. Xie, R. Finkelstein, J. P. Covey, J. S. Cotler, D. K. Mark, H.-Y. Huang, A. Kale *et al.*, Preparing random states and benchmarking with many-body quantum chaos, Nature (London) **613**, 468 (2023).

[22] J. S. Cotler, D. K. Mark, H.-Y. Huang, F. Hernández, J. Choi, A. L. Shaw, M. Endres, and S. Choi, Emergent quantum state designs from individual many-body wave functions, PRX Quantum **4**, 010311 (2023).

[23] See Supplemental Material at http://link.aps.org/supplemental/10.1103/PhysRevResearch.6.L032030 for details of the numerical simulations [28,37,38], the spin state ensemble at various rf driving times, analysis of power-law scaling in the superfluid velocity field [29], the process of magnetic domain formation, and the model of $\delta_{\rm th}(D)$.

[24] The second moment of any arbitrary observable $\mathcal{O}$ can be estimated with $\rho_{\mathcal{E}}^{(2)}$ as $\mathcal{O}^{(2)} = \sum_{\zeta\sim\mathcal{E}}(\boldsymbol{\zeta}^\dagger\mathcal{O}\boldsymbol{\zeta})^2 = \mathrm{tr}(\rho_{\mathcal{E}}^{(2)}\mathcal{O}^{\otimes 2})$.

[25] W. W. Ho and S. Choi, Exact emergent quantum state designs from quantum chaotic dynamics, Phys. Rev. Lett. **128**, 060601 (2022).

[26] M. Ippoliti and W. W. Ho, Dynamical purification and the emergence of quantum state designs from the projected ensemble, PRX Quantum **4**, 030322 (2023).

[27] The size of the system is $160\xi_s \times 160\xi_s$, covered by a 256×256 grid of equally spaced points, where $\xi_s \simeq 2.3\,\mu$m. See Supplemental Material [23] for details.

[28] P. B. Blakie, A. Bradley, M. Davis, R. Ballagh, and C. Gardiner, Dynamics and statistical mechanics of ultra-cold Bose gases using c-field techniques, Adv. Phys. **57**, 363 (2008).

[29] K. Fujimoto and M. Tsubota, Spin-superflow turbulence in spin-1 ferromagnetic spinor Bose-Einstein condensates, Phys. Rev. A **90**, 013629 (2014).

[30] S. Knoop, T. Schuster, R. Scelle, A. Trautmann, J. Appmeier, M. K. Oberthaler, E. Tiesinga, and E. Tiemann, Feshbach spectroscopy and analysis of the interaction potentials of ultracold sodium, Phys. Rev. A **83**, 042704 (2011).

[31] In the imaging, the spin axis $\hat{\boldsymbol{z}}$ was adiabatically rotated to the spatial axis $\hat{\boldsymbol{z}}'$.

[32] K. Fujimoto and M. Tsubota, Counterflow instability and turbulence in a spin-1 spinor Bose-Einstein condensate, Phys. Rev. A **85**, 033642 (2012).

[33] K. Fujimoto and M. Tsubota, Spin turbulence with small spin magnitude in spin-1 spinor Bose-Einstein condensates, Phys. Rev. A **88**, 063628 (2013).

[34] D. I. Bradley, S. N. Fisher, A. M. Guénault, R. P. Haley, G. R. Pickett, D. Potts, and V. Tsepelin, Direct measurement of the energy dissipated by quantum turbulence, Nat. Phys. **7**, 473 (2011).

[35] S. P. Thampi and J. M. Yeomans, Active turbulence in active nematics, Eur. Phys. J. Spec. Top. **225**, 651 (2016).

[36] R. Alert, J. Casademunt, and J.-F. Joanny, Active turbulence, Annu. Rev. Condens. Matter Phys. **13**, 143 (2022).

[37] X. Antoine and R. Duboscq, GPELab, a Matlab toolbox to solve Gross-Pitaevskii equations II: Dynamics and stochastic simulations, Comput. Phys. Commun. **193**, 95 (2015).

[38] A. Polkovnikov, Phase space representation of quantum dynamics, Ann. Phys. **325**, 1790 (2010).